Front. Earth Sci. 2022, 16(1): 99–108
https://doi.org/10.1007/s11707-021-0902-0

RESEARCH ARTICLE

Consistency correction of echo intensity data for multiple radar systems and its application in quantitative estimation of typhoon precipitation

Shuai ZHANG (✉)[1,2,5,6], Jing HAN[3,4], Bingke ZHAO[1], Zhigang CHU[2], Jie TANG[1], Limin LIN[1], Xiaoqin LU[1], Jiaming YAN[1]

1 Shanghai Typhoon Institute, China Meteorological Administration, Shanghai 200030, Chin
2 Collaborative Innovation Center on Forecast and Evaluation of Meteorological Disasters, Key Laboratory for Aerosol-Cloud-Precipitation (China Meteorological Administration), Nanjing University of Information Science & Technology, Nanjing 210044, China
3 Hainan Institute of Meteorological Sciences, Haikou 570203, China
4 Key Laboratory of South China Sea Meteorological Disaster Prevention and Mitigation of Hainan Province, Haikou 570203, China
5 Fujian Key Laboratory of Severe Weather, Fuzhou 350001, China
6 Fujian Key Laboratory of Granular Computing and Application, Minnan Normal University, Zhangzhou 363000, China

Abstract Calibration error is one of the primary sources of bias in echo intensity measurements by ground-based radar systems. Calibration errors cause data discontinuity between adjacent radars and reduce the effectiveness of the radar system. The Global Precipitation Measurement Ku-band Precipitation Radar (GPM KuPR) has been shown to provide stable long-term observations. In this study, GPM KuPR observations were converted to S-band approximations, which were then matched spatially and temporally with ground-based radar observations. The measurements of stratiform precipitation below the melting layer collected by the KuPR during Typhoon Ampil were compared with those of multiple radar systems in the Yangtze River Delta to determine the deviations in the echo intensity between the KuPR and the ground-based radar systems. The echo intensity data collected by the ground-based radar systems was corrected using the KuPR observations as reference, and the correction results were verified by comparing them with rain gauge observations. It was found that after the correction, the consistency of the echo intensity measurements of the multiple radar systems improved significantly, and the precipitation estimates based on the revised ground-based radar observations were closer to the rain gauge measurements.

Keywords calibration error, ground-based radar, reflectivity, correction, precipitation estimates

Received July 17, 2020; accepted April 19, 2021

E-mail: zhangs@typhoon.org.cn

1 Introduction

Typhoons are the strongest rainfall-generating weather systems in nature. All record-breaking torrential rains in China have been caused by typhoons (Tao, 1980). The most extensive damage during tropical cyclones is often the result of secondary disasters, such as heavy rainstorms and the consequent flash floods and landslides (Chen and Ding, 1979; Yu and Chen, 2019). Zhang et al. (2010) have analyzed the impact of all typhoons that made landfall in Chinese mainland from 2001 to 2007, and found that the damage caused by heavy rainstorms was often more serious than that due to excessive winds. This indicates that the impact of heavy rainfall is more significant than that of the wind power when typhoons make landfall. With the continuous urbanization, many urban areas in China face an increasingly serious problem of waterlogging due to typhoon-induced precipitation (Duan et al., 2016; Shi, 2016; Xu et al., 2016). As a result, research on the monitoring and impact assessment of typhoon-induced precipitation has gained widespread attention (Chen et al., 2004; Li et al., 2005; Dong et al., 2009; Nasrollahi et al., 2012; Wang et al., 2015a). Reliable spatial–temporal distribution data of precipitation are critical when analyzing the type, intensity, and trends of precipitation (Cheng et al., 2005). Therefore, better observation and research methods of typhoon precipitation are essential for improving the understanding of the distribution and its impact of typhoon-induced precipitation.

The new generation weather radar systems can generate precipitation estimation products at an extremely high

spatial–temporal resolution, making them a superior tool for mesoscale meteorological studies. The observations of single ground-based weather radar are affected by the Earth's curvature, which implies that the radar cannot detect targets at a long range or when solid obstacles present within its range. Consequently, single-radar systems are unsuitable for detecting large-scale weather systems and have a very limited application in the early-warning systems for disaster weather, such as those that monitor and predict the development and movement of typhoons. In contrast, multiple radar systems cannot only provide a greater detection range, allowing for more intuitive and convenient analysis of large-scale systems but also compensate, to a certain extent, for the disadvantages of single-radar systems, such as the existence of the cone of silence or the decreasing angular resolution as the slant range increases.

Because the estimation of precipitation from weather radar observations involves making assumptions regarding the size distribution and the evolution of hydrometeor particles from the observation height to the ground, the precipitation forecast has some uncertainties associated with it. However, the most fundamental uncertainty is related to the reliability of radar observations (Warren et al., 2018). The reliability of weather radar data is affected not only by common external factors, such as super-refraction and ground clutter, but also by the accuracy of the reflectivity data itself. The equivalent reflectivity factor Z can be obtained from the average echo power $\overline{P}_r$ at a distance r from the radar (Zhang et al., 2000):

$$Z = Cr^2\overline{P}_r, \tag{1}$$

where C is the radar constant related to the transmitting power, transmitting wavelength, beam width, pulse width, and the antenna gain of the radar. Taking the common logarithm of Eq. (1) and multiplying both sides by 10 gives the reflectivity factor value in dBZ:

$$\hat{Z} = \hat{C} + 2\hat{r} + \hat{P}_r, \tag{2}$$

where $\hat{Z} = 10\log_{10}Z$, and $\hat{C}$, $\hat{r}$, and $\hat{P}_r$ can be obtained in the same way. It is evident from Eq. (2) that any error in $\hat{C}$ will cause an equivalent error in the reflectivity factor. Therefore, when using the Z–I relationship to estimate precipitation, inaccuracies in the radar calibration constant C might result in significant estimation errors. The empirical quantitative precipitation estimation model can be expressed in logarithmic form $Z = 10 \times \log_{10}(a) + 10 \times b \times \log_{10}(R)$. If the error caused by the model is ignored, the formula can be differentiated to $\Delta Z = \frac{10b}{\ln 10}\frac{\Delta R}{R}$. The relative error of quantitativeprecipitation estimation $\left(\frac{\Delta R}{R}\right)$ is linear with ΔZ. If the value of b is between 1.4 to 1.6, when ΔZ is 3 dB, the relative error of quantitative precipitation estimation will reach 40% to 60%.

There are many calibration methods to maintain accurate radar measurement of single radar. CINRAD systems use internally generated test signals to calibrate reflectivity for every volume scan (Zhang et al., 2000), but it's difficult to obtain full-path errors including receiver, transmitter, antenna and wave guides. The standard floating metal ball method is neither easy to operate nor to be frequently used (Atlas, 2002). The method of reference rain gauge or rain gauge is feasible for qualitative assessment, but it is not acceptable for quantitative calibration due to the spatiotemporal variability and different observation results (Vaccarono et al., 2016).

The precipitation estimation range is limited when using a single radar system due to beam broadening, with the effective radius usually measuring $\leqslant$100 km. Consequently, quantitative precipitation estimation using multiple ground-radars is widely used for large-scale precipitation products. In applications of networked radars, the calibration error can cause the echo intensity data discontinuous, and lead to inconsistencies of quantitative precipitation estimation results (Zhang et al., 2011). Smith et al. (1996) analyzed the precipitation estimates from the weather radars at Tulsa and Twin Lakes, Oklahoma, United States, and found that the precipitation estimates varied in the overlap areas due to the different calibration errors, with the mean precipitation of the Tulsa radar being 30% higher than that at the Twin Lakes radar. Xiao et al. (2006) compared two adjacent S-band operational radars in south China and found that the reflectivity deviation in the overlapping area reached 3 dB; they also analyzed echo intensity data of five radars from the middle and lower reaches of the Yangtze River, and found that Wuhan radar's echo intensities are 2.4 dB weaker than that of Hefei radar, 4.6 dB lower than Yichang, and 2.4 dB lower than Changsha (Xiao and Liu, 2007). Han et al. (2018) compared three S-band radars in southern Jiangsu and found that Nanjing radar was about 3.5 dB weaker than that of Changzhou radar which is about 0.9 dB weaker than reflectivity of Nantong radar. Although the inter-calibration between adjacent ground radars is reliable, it is difficult to determine which radar is more accurate. The Precipitation Radar (PR) on board of the Tropical Rainfall Measuring Mission (TRMM), launched in 1997, provided three-dimensional precipitation data with a wide coverage; and the PR covered the areas of China below the latitude of 38°N (Iguchi et al., 2000; Kozu et al., 2001; Liao et al., 2001). The coverage of the TRMM's successor-the Global Precipitation Measurement (GPM) mission extends to the North and South Arctic Circles (Hou et al., 2014). The GPM satellite radar has been accurately calibrated using the US GPM Ground Validation System to an error of less than 1dB (Iguchi et al., 2016). It has been operating steadily for many years, generating consistent and highly reliable data (Warren et al., 2018). A few researchers have compared the reflectivity data of the GPM Dual-Frequency

Precipitation Radar (DPR) against the observations of dual-polarization ground-based radars (GRs) in the southeastern United States and found that the overall performance of the GPM DPR was satisfactory (Iguchi et al., 2016; Biswas and Chandrasekar, 2018). Chu et al. (2018) reduced the calibration errors by referring the Ku-Band Precipitation Radar (KuPR) carried by the Global Precipitation Measurement (GPM) Core Observatory as a standard reference, and the spatial continuity of reflectivity factor and precipitation estimation fields of three radar covering the lower reaches of the Yangtze in China Yangzi was significantly improved after bias correction. Warren et al. (2018) compared observations from multiple radars in Sydney, Australia collected in 2009–2015 with satellite radar data (TRMM PR and GPM Ku-band PR) to quantify the calibration errors of the ground radars and verify the attenuation correction algorithm, indicating that the GPM Ku-band PR has been providing well-calibrated and stable observations. The GPM KuPR observations form a homogenous, continuous, and stable data set. In recent years, the wide coverage and good calibration data of space-borne radar has been widely used by researchers, and is used as a reference to estimate the calibration error of ground-based radars (Liao et al., 2001; Liao and Meneghini, 2009; Han et al., 2018).

Reducing calibration errors and mitigating spatial discontinuity are equally important for multiple radar systems' QPEs (Quantitative Precipitation Estimation). The objective of this study is to improve QPEs of networked radars by discontinuity correction. This paper is organized as follows: Section 2 introduces the data and approaches used in this research, Section 3 analyze the consistency and correct the observations of a multiple radar systems consisting of three radars (Nantong (NT), Shanghai Qingpu (QP), and Zhoushan (ZS)) located in the Yangtze River Delta region, by comparing the networked radars' observations with the GPM KuPR data collected during typhoon Ampil, which landed in Shanghai in 2018. In section 4, the quantitative precipitation estimation results of the networked radars before and after applying the correction were analyzed using ground precipitation gauge measurements to verify the correction.

2 Data and methods

2.1 Echo intensity data of the space-borne radar

The GPM KuPR and the TRMM/PR parameters are essentially the same (Awaka et al., 2016). In this study, the GPM KuPR was selected as the reference standard for the correction of the ground-based radars' observation because it has a longer wavelength than the Ka-band PR, making it more compatible with the GR system. Although the Ka-band PR is not directly used in this study, some of its observations have been utilized in the attenuation correction, bright band detection, and echo classification algorithms for the GPM KuPR (Ma et al., 2020). The GPM KuPR data are contained in the V05 version of the L2 product, and they include the attenuation-corrected 3D reflectivity, precipitation type, and bright band parameters. The data can be downloaded through the Precipitation Processing System of the Goddard Space Flight Center (available at NASA website). Similar to TRMM, the GMP L2 products undergo quality control, beam-filling correction, near-surface clutter suppression, and attenuation correction. Because it is based on a dual-frequency algorithm, the attenuation correction method for the L2 products (Meneghini et al., 2015; Seto and Iguchi, 2015) is better than that used for the TRMM PR products.

2.2 Ground-based weather radar (GR) data

In this study, we selected three S-band weather radars (China New Generation Weather Radar (CINRAD)) located in the following three areas of the Yangtze River Delta: Nantong (NT), Shanghai Qingpu (QP), and Zhoushan (ZS). The effect of attenuation on the S-band radar data can be ignored. The temporal resolution of the echo intensity data is 6 min, horizontal resolution is $1° \times 1°$ km, and data are recorded in polar coordinates. This study uses the reflectivity factor data acquired by the multiple radar systems during typhoon Ampil in 2018. Clear air echo filtering and Severe Weather Now-casting System quality control was used to eliminate non-precipitation echo from the data (Wu et al., 2013). Areas where the radar beam was blocked were identified manually.

2.3 Precipitation measurement data

In this study, hourly rain gauge data was used as reference data. Although rain gauge data are affected by sampling errors due to different factors, such as calibration, wind, and evaporation (Ma et al., 2015), and they can still be considered as representative data of precipitation (Francisco et al., 2012). To verify the corrected reflectivity factor data, we selected rain gauge data within 100 km of the three netted-system radars during the duration of typhoon Ampil. There are two OTT disdrometers deployed in Pudong, Shanghai. The disdrometers could measure rain DSD and fall velocities for particle size from 0.3 to 20 mm (Chu et al., 2018), they are used here to derive Z (reflectivity factor)-R (rain rate) relationship for typhoon precipitations.

2.4 Spatial and temporal matchup

The GPM mission is an international satellite mission to provide accurate precipitation measurements around the globe every 2 to 4 h (available online at NASA website) (Chandrasekar et al., 2008). A complete volume scan of the

GR is approximately 6 min; therefore, the time window for matching the KuPR data and the GR data are also ±6 min. There may be more than one obtained volume scans during any given 6-min interval, to minimize the time difference, we select the KuPR data based on the observation area and then select the GR scan data that most closely matches the KuPR detection time.

The geometric intersection method was used to match the KuPR and the GR data spatially (Wang et al., 2015b). To limit the effect of beam broadening, the matching range was limited to a distance of 100 km from the ground-based radar (Zhu et al., 2016). Because the minimum detectable signal strength of the KuPR is about 18 dBZ (Seto and Iguchi, 2015), whereas the GR can detect signals with much lower reflectivity, a detection threshold of 15 dBZ was selected to minimize the differences between the PR and GR observations (Morris and Schwaller, 2011). In the geometric intersection method, the two types of radar data are matched spatially by calculating the mean reflectivity factor and the GR reflectivity factor at the geometric intersection of the Ku-band scan and each GR sweep surface (as shown in Fig. 1). Therefore, the horizontal resolution of the matched data is consistent with that of the KuPR data, and the vertical resolution is consistent with that of the GR reflectivity factor data (Kim et al., 2014).

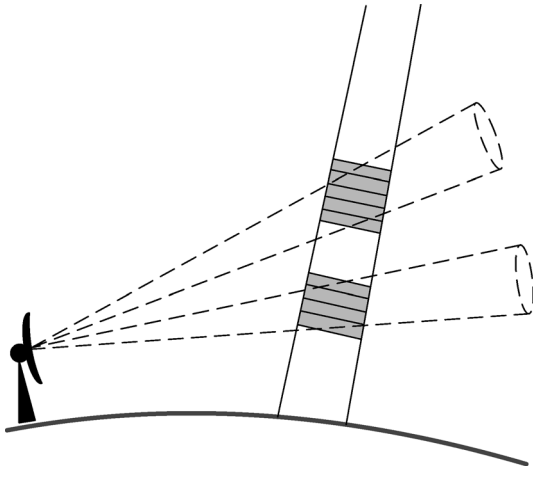

Fig. 1 Schematic illustration of the geometry-matching method (Solid lines represent the KuPR scanning beam; dashed lines represent the GR sweeps; shading represents the overlap area) (Goddard Space Flight Center, 2014).

3 Analysis of echo intensity differences between networked radars

The severe tropical storm Ampil was formed on the northwestern Pacific Ocean about 680 km east of Luzon Island in the Philippines on the morning of July 18. In the early morning of July 21, it crossed Okinawa Island and entered the East China Sea, gradually approaching the east China coast. It made landfall along the coast of Chongming Island in Shanghai at July 22 (Fig. 2), with the maximum wind speed of 28 m/s (tenth level) near the center and the lowest pressure of 982 hPa in the center. After what, it rapidly weakened into a tropical storm.

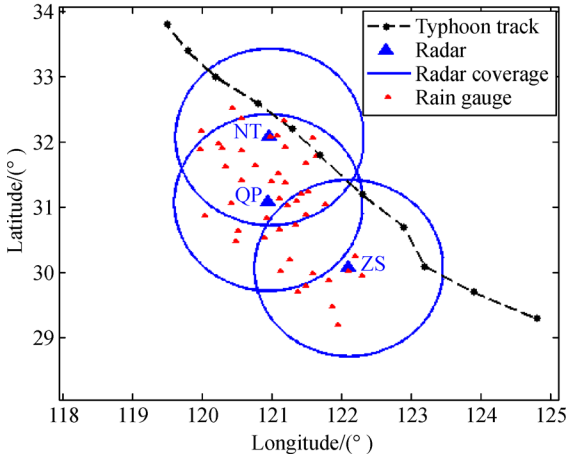

Fig. 2 The best track of typhoon Ampil (from 23:00, July 21 to 05:00, July 23, 2018 (UTC + 8)), effective precipitation observation range (150 km) of the three radars and rain gauge stations.

The movement of Typhoon Ampil in the offshore region was monitored by the three radars (Fig. 3). As indicated by the mosaic of the three radars, the structural integrity of Typhoon Ampil had already been compromised as it approached landfall. The primary and secondary rain belts merged and evolved into a large rain belt, and the strong echo area was distributed along the rain belt near the center of the typhoon, whereas the overall structure maintained the spiral pattern. The three-radar 1-km mosaic showed that NT radar and QP radar received similar echo

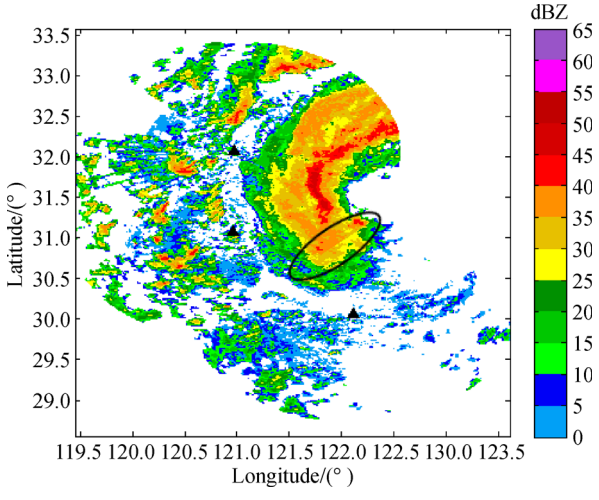

Fig. 3 The three-radar mosaic of the echo intensity at 1-km height before correction (NT, QP, and ZS radar) at 02:30, July 22, 2018 (UTC), the black triangles represent the locations of the radars, and the black ellipse highlights the discontinuity area.

intensities; however, there was a clear discontinuity between the echo intensities of ZS radar and QP radar (the black ellipse in Fig. 3). Compared with QP radar, the echo intensity received by ZS radar was obviously weaker.

The echo intensity data of two adjacent radars can be compared to quantify the observation deviations between them (Liu et al., 2002). The impact of ground clutters and radar data interpolation at high elevation angles on the observation deviations should be minimized so that the deviations can essentially affected by systematic differences only. To this end, a spatial region resembling a "floating cylinder" (Fig. 4) is selected for radar observation comparison. The cylinder axis overlaps with the mid-perpendicular line of the horizontal line segment connecting the two GRs, and the base radius is 10 km, with the top and bottom bases at 1.5 and 10 km above the mean sea level (MSL), respectively.

The time series of the mean echo intensity and deviations in the mean are presented in Fig. 5. It shows that the three radars basically have the same trend in time series of echo intensity. The echo intensity deviations between radars fluctuate with time, which may be related to the random changes in radar constants and the errors in spatiotemporal matching. The radar reflectivity factor (referred to as Z and expressed in dBZ) of ZS radar is significantly smaller than that of NT radar, whereas the latter is very close to that of QP radar (refer to Table 1 for the biases and standard deviations).

Table 1 Statistics of the deviations of echo intensity between NT and QP radar, NT and ZS radar

NT-QP	Bias/dB	−0.436
	σ	0.258
NT-ZS	Bias/dB	5.486
	σ	0.519

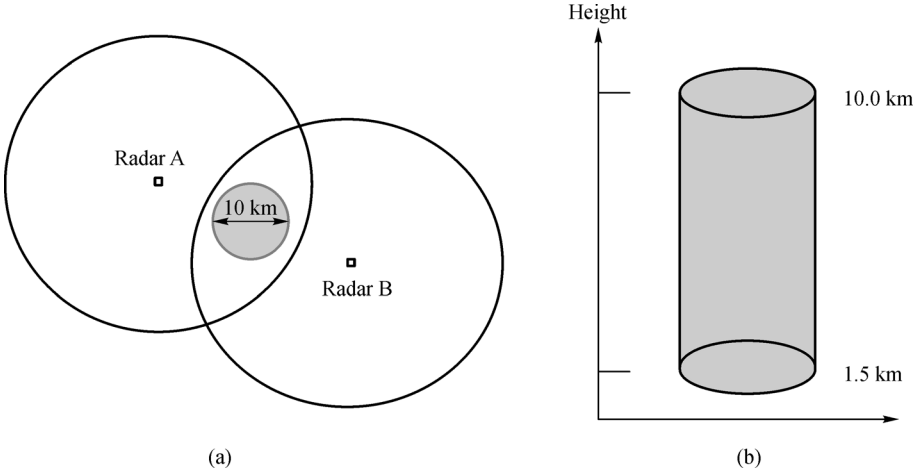

Fig. 4 Sketch of the "floating cylinder" for data comparison between two adjacent ground-based radars.

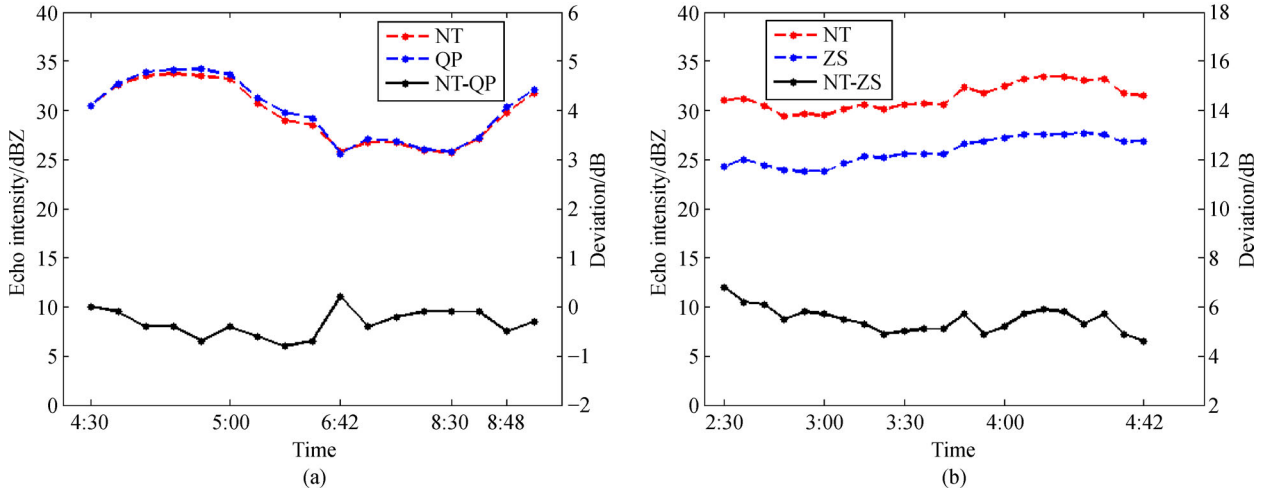

Fig. 5 Time series of the reflectivity factors of the three radars and deviations between QP, ZS, and NT radar. (a) NT radar vs. QP radar; (b) NT radar vs. ZS radar. The black lines represent the deviations.

4 GPM KuPR-based correction and verification

4.1 Data selection for comparison

To reduce the above-mentioned deviations, the bias was corrected by using the KuPR data as reference. Considering that the KuPR and GRs differ from each other in several aspects such as working frequency, scanning method, viewing angle, sampling volume, and resolution, the radar data should be first corrected for such differences before being subjected to statistical analysis.

The main procedures are as follows:

1) Handling of ground obstacles of GRs

Among the three GRs, the ground obstacles of Nantong radar are at azimuth angles of 167°–172° and 211°–218° when the elevation angle is 0.5°, and 211°–218° when the elevation angle is 1.5°.

2) Selection of GR radial distance

Analysis shows that GR and KuPR observations are affected by ground objects in the radial distance of 0–25 km, whereas GR beams undergo severe broadening when more than 100 km away in the radial direction. Therefore, data matching is only performed in the radial distance range of 25–100 km (Warren et al., 2018).

3) Ku-band adjustment

The KuPR operates in the Ku band whereas GRs operate in the S band. Different wavelengths have different Mie scattering effects, which may make it impossible to directly compare Z between the two types of radars. To overcome this problem, Ku-band adjustment is performed following Liao and Meneghini (2009), which converts echo intensities detected by radars of different beam wavelengths into echo intensities of the same wavelength, while selecting as many matching points as possible with a high degree of filling, to minimize the influence of non-uniform beam filling (NUBF) (Zhang et al., 2019).

4) Selection of height

According to Zhang et al. (2019), the KuPR and an S-band GR have a relatively stable deviation in the observations of stratiform precipitation, and the observation correlation between the two radars is higher below the melting layer than that above the melting layer. Therefore, the reflectivity factors of stratiform precipitation below the melting layer are selected to analyze the observation deviations between the two types of radar.

4.2 Bias correction

Three statistics of the echo intensity data between the three GRs and KuPR were calculated after the above procedures, namely the mean bias (Bias), standard deviation (σ), and correlation coefficient (CC). True Z relates to its measured value Z_{m} as follows:

$$Z_{\mathrm{m}} = Z + \Delta Z. \tag{3}$$

Using the KuPR data as reference, the bias of the three GRs in Z value can be calculated using Eq. (2):

$$\Delta Z = Z_{\mathrm{KuPR}} - Z_{\mathrm{GR}}, \tag{4}$$

where ΔZ are expressed in dB. The results (Table 2) show that Z was negatively biased by approximately 1.97 dB, 1.42 dB, and 7.27 dB for Nantong radar, Qingpu radar, and Zhoushan radar, respectively. N is the number of matching points in the scan regions of the KuPR and the GR, σ is the standard deviation, and CC is the correlation coefficient in Table 2. It can also be seen from Table 2 that the deviation between NT radar and ZS radar is about 5.3 dB, and the deviation between NT radar and QP radar is about −0.5 dB. The results are very close to the values in Table 1 which obtained by comparing reflectivity factors between adjacent radars. So, the accuracy of the results in Table 2 can be considered reliable.

The GR echo intensities were corrected using the Z biases with respect to the KuPR. As shown in Fig. 6, the observation consistency between the three GRs is significantly improved after correction as opposed to before correction (Fig. 3). The mean echo intensity deviations between NT and QP, Nantong and ZS were reduced to 0.16 and 0.15 dB, respectively.

Table 2 Statistics of the reflectivity factor deviations between the three GRs and the KuPR on July 22, 2018, during typhoon Ampil

NT	Bias/dB (GR-PR)	−1.967
	σ	2.252
	CC	0.864
	N	10389
QP	Bias/dB (GR-PR)	−1.421
	σ	2.286
	CC	0.868
	N	3202
ZS	Bias/dB (GR-PR)	−7.265
	σ	2.620
	CC	0.81
	N	1149

4.3 Verification of the correction

4.3.1 Applicability verification in typhoons

Tropical storm Jongdari reached typhoon level at 20:00 on July 26, and made landfall in Jinshan District, Shanghai at about 10:30 on August 3, was about 10 days from the last typhoon Ampil that landed in Chongming District, Shanghai. As indicated by Fig. 7, the echo intensity of ZS radar was obviously weaker than that of the other two radars, which is similar to Fig. 3.

Figure 8 shows the deviations between the three radars.

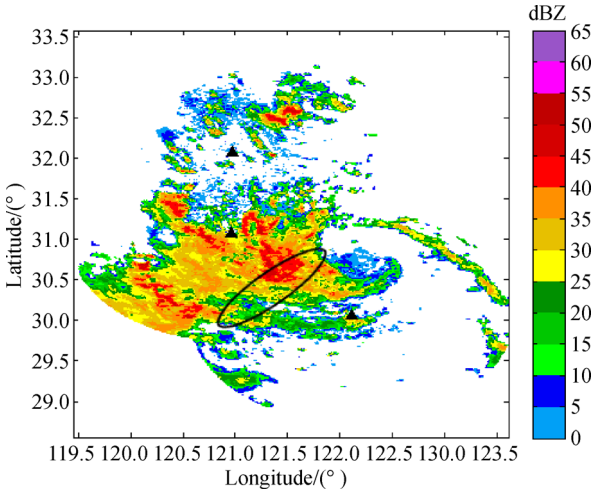

Fig. 6 The three-radar mosaic of the echo intensity at 1-km height after the correction (NT, QP, and ZS radar) at 02:30, July 22, 2018 (UTC), the black triangles represent the locations of the radars.

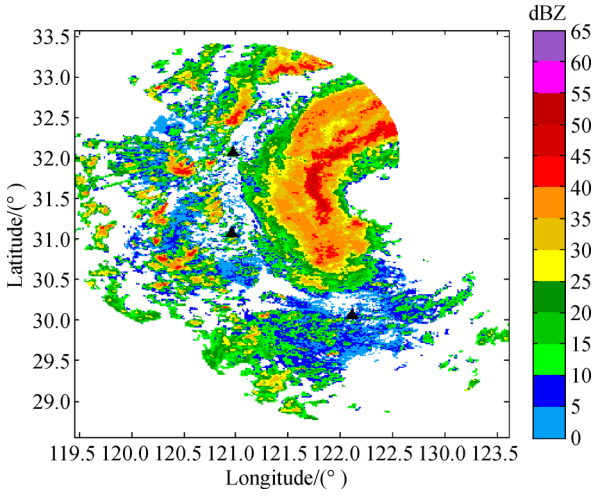

Fig. 7 The three-radar mosaic of the echo intensity at 1-km height before correction (NT, QP, and ZS radar) at 19:30, August 02, 2018 (UTC), the black triangles represent the locations of the radars, and the black ellipse highlights the discontinuity area.

The mean deviation of echo intensity between QP radar and ZS radar is 5.8 dB, and that between NT radar and ZS radar is 6.0 dB.The deviation is stable within 1dB compared with that during Typhoon Ampil. It can be considered that the above three radars were basically stable in the interval time between the two typhoons. The GRs' echo intensities were corrected using the biases with respect to the observations of KuPR in Table 2. The deviations between NT and ZS radar, QP and ZS radar were reduced to 0.71 and 0.04 dB respectively after correction, and the observation consistency between the three GRs was significantly improved (Fig. 9).

4.3.2 Correction accuracy verification

The gauge data was used for further analysis, the reflectivity factor data for positions corresponding to rain gauge stations was determined using the natural neighbor interpolation method. The echo intensities are converted to rainfall intensities using the empirical Z–I relationship $Z = aR^b$, and then the 1 h cumulative precipitation was estimated. Previous researches showed that the typhoon precipitations contain higher raindrop concentration and have lower raindrop diameter than that of maritime convection (Tokay et al., 2008; Wen et al., 2018; Bao

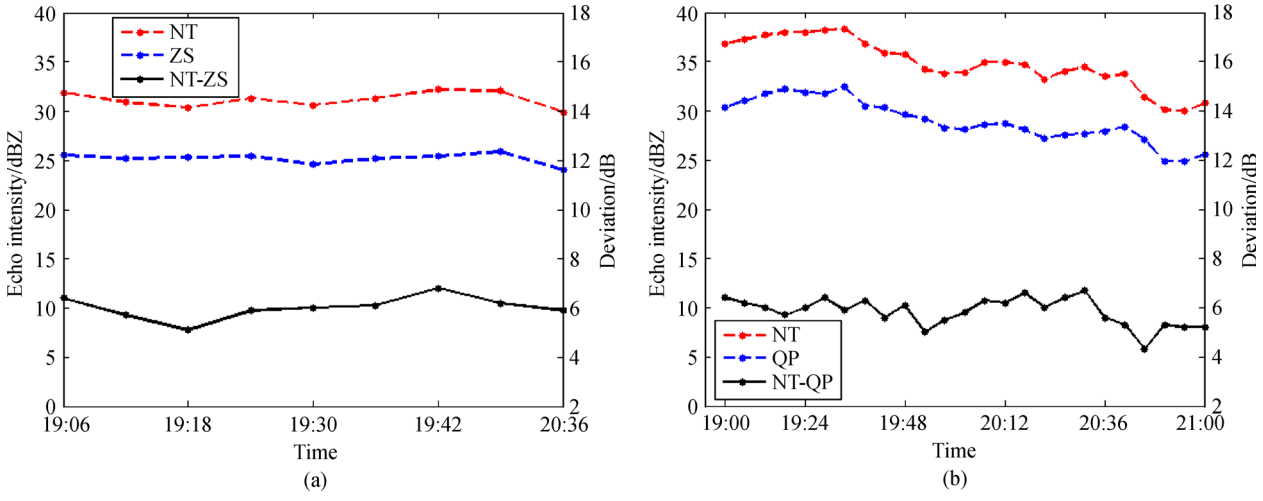

Fig. 8 Time series of the reflectivity factors of QP, ZS, and NT radars and time series of reflectivity factor differences between the radars. (a) NT radar vs. QP radar; (b) QP radar vs. ZS radar. The black lines represent the deviations.

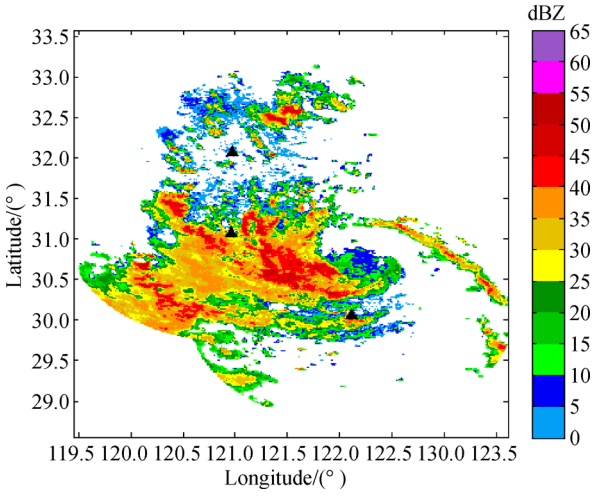

Fig. 9 The three-radar mosaic of the echo intensity at 1-km height after correction (NT, QP, and ZS radar) at 19:30, August 02, 2018 (UTC), the black triangles represent the locations of the radars.

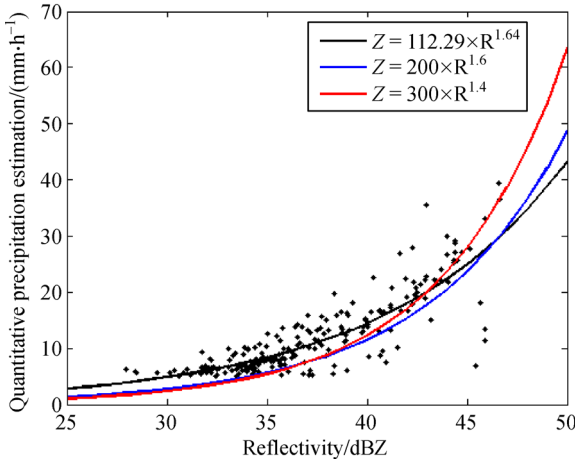

Fig. 10 The Z (reflectivity factor)-R (rain rate) relationship $Z = 112.29R^{1.64}$ derived from disdrometers deployed in Nanhui and Expo stations during Typhoon Ampil, and two commonly used relations.

et al., 2020). Raindrop size distributions (DSDs) are the fundamental microphysical property of precipitation. A Z (reflectivity factor)-R (rain rate) relationship $Z = 112.29R^{1.64}$ derived from disdrometers deployed in Nanhui and Expo stations during typhoon Ampil, as shown in Fig. 10. The quantitative precipitation estimations using Z was compared with the rain gauge data within 100 km of the three GRs. The statistics of the deviations between the rain gauge data and the radar-estimated precipitation before and after the correction are presented in Table 3, where Bias denotes the mean bias, σ is the standard deviation, and CC represents the correlation coefficient. The statistics shows that the radar-estimated precipitation after correction is closer to the rain gauge data than that before correction.

Table 3 Statistics of the deviations between rain gauge data and QPEs derived from the GRs' observation (NT, QP, and ZS) during Typhoon Ampil

Before correction	Bias/(mm·h^{-1}) (Gauge-QPE)	1.35
	σ/(mm·h^{-1})	2.94
	CC	0.89
After correction	Bias/(mm·h^{-1}) (Gauge-QPE)	0.61
	σ/(mm·h^{-1})	2.49
	CC	0.90

5 Discussion and conclusions

It's found that there are obvious discontinuities in the mosaic of the three S-band GRs in the Yangtze River Delta region (NT, QP in Shanghai, and ZS radar) during the impact period of Ampil in 2018. The echo intensities of the three GRs are subjected to consistency analysis and correction using the GPM KuPR data. The correction reliability was verified using the gauge data. The results show that:

1) NT and QP radars receive similar echo intensities. The reflectivity factor of ZS radar is obviously smaller than that of NT radar by more than 5 dB, which is the reason of the discontinuity in the 1-km mosaic.

2) After correction, the Z differences between the radars are significantly decreased, thereby significantly improving the echo intensity mosaic of the three GRs, demonstrating an improved consistency in echo intensity of multiple radar systems.

3) After correction, the rainfall estimated using the three radars' echo intensities are closer to the rain gauge data, indicating that the GPM KuPR-based correction of echo intensity consistency improves the accuracy of rainfall prediction by multiple radar systems.

Restricted by the observation mode of the GPM satellite, the space-borne radar only samples at limited times in the scan regions of GRs, which means that there will be few matching events in general and even fewer matching events of non-precipitation echoes and precipitation echoes in particular, thereby making it impossible to achieve a real-time comparison of observation data between the satellite-borne radar and the GRs. A hybrid method is used to correct for attenuation of the KuPR beam (Meneghini et al., 2015), which can be significant in heavy rainfall. It means that there may be errors in the KuPR data when heavy rainfall occurs.

For the rain gauges, the collection of rain suffers from the wind-induced under-catch caused by trajectory deflection due to flow distortions. The observation values by the

gauges may be smaller than the true values, and further long-term experiments are needed to obtain the gauge catch ration under typhoon conditions. The typhoon precipitations contain higher raindrop concentration and lower raindrop diameter than that of maritime convections, and have complex structure. Limited by the number of raindrop spectrometers, the data used in this study is limited in the interpretation of the precipitation structure.

Acknowledgements This work was supported by the Key Projects of the National Key R&D Program (No. 2018YFC1506303), the Key Program for International S&T Cooperation Projects of China (No. 2017YFE0107700), the National Natural Science Foundation of China (Grant Nos. 41775064 and 41806046), Shanghai Natural Science Foundation (No. 21ZR1477300), and Fujian Key Laboratory of Severe Weather Open Foundation (No. 2020TFS02).

References

Atlas D (2002). Radar calibration: some simple approaches. Bull Am Meteorol Soc, 83(9): 1313–1316

Awaka J, Le M, Chandrasekar V, Yoshida N, Higashiuwatoko T, Kubota T, Iguchi T (2016). Rain type classification algorithm module for GPM dual-frequency precipitation radar. J Atmos Ocean Technol, 33 (9): 1887–1898

Bao X W, Wu L G, Zhang S, Li L M, Zhao B K (2020). Distinct raindrop size distributions of convective inner-and outer-rainband rain in Typhoon Maria (2018). J Geophys Res Atmos, 125e2020JD032482

Biswas S, Chandrasekar C V (2018). Cross-validation of observations between the GPM dual-frequency precipitation radar and ground based dual-polarization radars. Remote Sens, 10(11): 1773

Chandrasekar V, Hou A, Smith E, Bringi V N, Rutledge S A, Gorgucci E, Petersen W A, Jackson G S (2008). Potential role of dual-polarization radar in the validation of satellite precipitation measurements: rationale and opportunities. Bull Am Meteorol Soc, 89(8): 1127–1146,

Chen L S, Luo Z X, Li Y (2004). Research advances on tropical cyclone landfall progress. Acta Meteorol Sin, 62: 541–549

Chen L, Ding Y (1979). An Introduction to the Western Pacific Typhoon. Beijing: Science Press, 1–491 (in Chinese)

Cheng Z Q, Chen L S, Xu X D (2005). Research progress on typhoon heavy rainfall in China for last ten years. Meteorol Mon, 31(12): 3–9 (in Chinese)

Chu Z, Ma Y, Zhang G, Wang Z, Han J, Kou L, Li N (2018). Mitigating spatial discontinuity of multi-radar QPE based on GPM/KuPR. Hydrology, 5(3): 48

Dong M Y, Chen L S, Zheng P Q (2009). Research progress on abrupt intensification of heavy rainfall and super heavy rainfall associated with landfalling tropical cyclones. J Trop Meteorol, 25: 495–502 (in Chinese)

Duan W L, He B, Nover D, Fan J, Yang G, Chen W, Meng H, Liu C (2016). Floods and associated socioeconomic damages in China over the last century. Nat Hazards, 82(1): 401–413

Francisco J T, Turk F J, Petersenc W, Hou A Y, García-Ortegae E, Machado L A T, Angelis C F, Salio P, Kidd C, Huffman G J, de Castroa M (2012). Global precipitation measurement: methods, datasets and applications. Atmos Res, 104–105(1): 70–97

Goddard Space Flight Center (2014). Validation Network Data Product User's Guide Volume 1-TRMM Data Products. Available online at NASA website

Han J, Chu Z G, Wang Z H, Xu D, Li N, Kou L, Xu F, Zhu Y Q (2018). The establishment of optimal ground-basedradar datasets by comparison and correlation analyses with space-borne radar data. Meteorol Appl, 25(1): 161–170

Hou A Y, Kakar R K, Neeck S, Azarbarzin A A, Kummerow C D, Kojima M, Oki R, Nakamura K, Iguchi T (2014). The global precipitation measurement mission. Bull Am Meteorol Soc, 95(5): 701–722

Iguchi T, Kozu T, Meneghini R, Awaka J, Okamoto K (2000). Rain-profiling algorithm for the TRMM precipitation radar. J Appl Meteorol, 39(12): 2038–2052

Iguchi T, Seto S, Awaka J, Meneghini R, Kubota T, Oki R, Chandra V, Kawamoto N (2016). Performance of the dual-frequency precipitation radar on the GPM core satellite. Geophys Res Abstr, 18: EGU2016–EGU11581

Kim J H, Ou M L, Park J D, Morris K R, Schwaller M R, Wolff D B (2014). Global precipitation measurement (GPM) ground validation (GV) prototype in the Korean Peninsula. J Atmos Ocean Technol, 31 (9): 1902–1921

Kozu T, Kawanishi T, Kuroiwa H, Kojima M, Oikawa K, Kumagai H, Okamoto K, Okumura M, Nakatsuka H, Nishikawa K (2001). Development of precipitation radar onboard the Tropical Rainfall Measuring Mission (TRMM) satellite. IEEE Trans Geosci Remote Sens, 39(1): 102–116

Li Y, Chen L S, Xu X D (2005). Numerical experiments of the impact of moisture transportation on sustaining of the landfalling tropical cyclone and precipitation. Chin J Atmos Sci, 29: 91–98

Liao L, Meneghini R (2009). Changes in the TRMM Version-5 and Version-6 precipitation radar products due to orbit boost. J Meteorol Soc Jpn, 87A: 93–107

Liao L, Meneghini R, Iguchi T (2001). Comparisons of rain rate and reflectivity factor derived from the TRMM precipitation radar and the WSR-88D over the Melbourne, Florida. J Atmos Ocean Technol, 18 (12): 1959–1974

Liu Z C, Li B, Zhai W Q (2002). The New Generation of Weather Radar System Environment and Operation Management. Beijing: China Meteorological Press: 102–104

Ma Y, Chandrasekar V, Biswas S K (2020). A Bayesian correction approach for improving dual-frequency precipitation radar rainfall rate estimates. J Meteorol Soc Japan, 98(3): 511–525

Ma Y, Zhang Y, Yang D, Farhan S B (2015). Precipitation bias variability versus various gauges under different climatic conditions over the Third Pole Environment (TPE) region. Int J Climatol, 35(7): 1201–1211

Meneghini R, Kim H, Liao L, Jones J A, Kwiatkowski J M (2015). An initial assessment of the surface reference technique applied to data from the dual-frequency precipitation radar (DPR) on the GPM Satellite. J Atmos Ocean Technol, 32: 2281–2296

Morris K R, Schwaller M R (2011). Sensitivity of space-borne and ground radar comparison results to data analysis methods and

constraints. In: 35th Conf on Radar Meteorology, Pittsburgh, PA, American Meteorological Society

Nasrollahi N, Agha K A, Li J L, Gao X, Hsu K, Sorooshian S (2012). Assessing the impacts of different WRF precipitation physics in hurricane simulations. Weather Forecast, 27(4): 1003–1016

Seto S, Iguchi T (2015). Inter-comparison of attenuation correction methods for the GPM dual-frequency precipitation radar. J Atmos Ocean Technol, 32(5): 915–926

Shi P J (2016). Natural Disasters in China. Beijing: Springy and Beijing Normal University Press: 1–103

Smith J A, Seo D J, Baeck M L, Hudlow M D (1996). An inter-comparison Study of NEXRAD Precipitation Estimates. Water Resour Res, 32(7): 2035–2045

Tao S Y (1980). Rainstorm in China. Beijing: Science Press (in Chinese)

Tokay A, Bashor P G, Habib E, Kasparis T (2008). Raindrop size distribution measurements in tropical cyclones. Mon Weather Rev, 136(5): 1669–1685

Vaccarono M, Bechini R, Chandrasekar C V, Cremonini R, Cassardo C (2016). An integrated approach to monitoring the calibration stability of operational dual-polarization radars. Atmos Meas Tech, 9(11): 5367–5383

Wang Y P, Cui X P, Ran L K (2015a). Diagnosis of dynamical parameters in torrential rain associated with typhoon “Bilis” in 2006. Chin J Atmos Sci, 39: 747–756 (in Chinese)

Wang Z H, Li S Y, Dai J H (2015b). Comparative case study on the observations between the space-borne radar and ground-based radar. Plateau Meteorol, 34(3): 804–814 (in Chinese)

Warren R A, Protat A, Siems S T, Ramsay H A, Louf V, Manton M J, Kane T A (2018). Calibrating ground-basedradars against TRMM and GPM. J Atmos Ocean Technol, 35(2): 323–346

Wen L, Zhao K, Chen G, Wang M, Zhou B, Huang H, Hu D, Lee W C, Hu H (2018). Drop size distribution characteristics of seven typhoons in China. J Geophys Res D Atmospheres, 123(12): 6529–6548

Wu T, Wan Y F, Wo W F, Leng L (2013). Design and application of radar reflectivity quality control algorithm in SWAN. Meteorol Sci Tech, 41(5): 809–817 (in Chinese)

Xiao Y J, Liu L P (2007). Study of method for interpolating data from weather radar network to 3D grid and mosaics. Acta Meteorol Sin, 64 (5): 647–657 (in Chinese)

Xiao Y J, Liu L P, Yang H P (2006). A contrast analysis of synchronous observations from regional radar network. Acta Meteorol Sin, 65(6): 919–927 (in Chinese)

Xu W, Zhuo L, Zheng J, Ge Y, Gu Z, Tian Y (2016). Assessment of the casualty risk of multiple meteorological hazards in China. Int J Environ Res Public Health, 13(2): 222

Yu H, Chen L (2019). Impact assessment of landfalling tropical cyclones: introduction to the special issue. Front Earth Sci, 13(4): 669–671

Zhang J, Howard K, Langston C, Vasiloff S, Kaney B, Arthur A, Van Cooten S, Kelleher K, Kitzmiller D, Ding F, Seo D J, Wells E, Dempsey C (2011). National mosaic and multi-sensor QPE (NMQ) system: description, results, and future plans. Bull Am Meteorol Soc, 92(10): 1321–1338

Zhang P C, Du B Y, Dai T P (2000). Radar Meteorology. Beijing: China Meteorological Press, 165–169

Zhang Q H, Wei Q, Chen L S (2010). Impact of landfalling tropical cyclones in mainland China. Sci Sinica Terrae, 40(7): 941–946 (in Chinese)

Zhang S, Wang Z H, Zhao B K, Chen Y C (2019). Using space-borne radar data to correcting calibration errors in ground-based radar. Clim Env Res, 24(5): 576–584 (in Chinese)

Zhu Y Q, Wang Z H, Li N (2016). Consistency analysis and correction for observations from the radar at Nanjing. Acta Meteorol Sin, 74(2): 298–308 (in Chinese)